

# Two-parameter superposable S-curves

Vijay Prakash S

Independent Researcher, Alappuzha, Kerala, India.

[prakash.vijay.s@gmail.com](mailto:prakash.vijay.s@gmail.com)

## Abstract

Straight line equation  $y = mx$  with slope  $m$ , when singularly perturbed as  $ay^3 + y = mx$  with a positive parameter  $a$ , results in S-shaped curves or S-curves on a real plane. As  $a \rightarrow 0$ , we get back  $y = mx$  which is a cumulative distribution function of a continuous uniform distribution that describes the occurrence of every event in an interval to be equally probable. As  $a \rightarrow \infty$ , the derivative of  $y$  has finite support only at  $y = 0$  resembling a degenerate distribution. Based on these arguments, in this work, we propose that these S-curves can represent maximum entropy uniform distribution to a zero entropy single value. We also argue that these S-curves are superposable as they are only parametrically nonlinear but fundamentally linear. So far, the superposed forms have been used to capture the patterns of natural systems such as nonlinear dynamics of biological growth and kinetics of enzyme reactions. Here, we attempt to use the S-curve and its superposed form as a statistical model. We fit the models on a classical dataset containing flower measurements of iris plants and analyze their usefulness in pattern recognition. Based on these models, we claim that any non-uniform pattern can be represented as a singular perturbation to uniform distribution. However, our parametric estimation procedure have some limitations such as sensitivity to initial conditions depending on the data at hand.

## 1 Introduction

Usually represented as a modified form of exponential function, sigmoidal or S-shaped pattern is observed in various scientific domains [1]. The sigmoidal function is given by

$$S_{\text{exp}}(x) = \frac{1}{1 + e^{-x}}. \quad (1)$$

Superposition of the above S-curve by Cybenko [2] has led to the development of universal function approximation by Hornik et al [3]. Other similar modified forms of exponential function include the logistic function and its extensions [4, 5, 6, 7].

Typically, S-curves are integrals of bell-shaped curves. De Moivre was the first to modify the exponential function to represent errors in measurements as bell-shaped curves [8]. De Moivre's modified form was later parametrized by Gauss now known as the normal distribution function given by

$$\tilde{y} = \frac{1}{\sqrt{2\pi}\sigma} \exp^{-\frac{1}{2}\left(\frac{x-\mu}{\sigma}\right)^2} \quad (2)$$

which are two-parameter family of curves. However, once the mean  $\mu$  is located the height and tails of the bell-curve is controlled by just one parameter  $\sigma$ . The above bell-curve  $\tilde{y}$  is the derivative of Gauss error function which is also an S-curve.  $\tilde{y} \rightarrow 0$  for both  $\sigma \rightarrow 0$  and  $\sigma \rightarrow \infty$ . So,  $\tilde{y}$  is applicable only for distributions with finite variance[9].

S-curves can also be obtained algebraically. A singular perturbation to the straight line equation  $y = mx$  also results in S-curves given by [10, 11]

$$y - y_c = \frac{m(x - x_c)}{1 + a(y - y_c)^2}, \quad (3)$$

where  $a$  and  $m$  are the parameters with  $(x_c, y_c)$  as the point of inflection. Corresponding bell-curves are given by

$$\frac{dy}{dx} = \frac{m}{1 + a(y - y_c)^2}. \quad (4)$$

At the point of inflection  $y = y_c$ ,  $\frac{dy}{dx} = m$ . Unlike Eqn. (2), a bell-curve described with the above equation has two parameters  $a$  and  $m$ . Its height is described by  $m$  and both  $a$  and  $m$  describe the tails.

The real solution of Eqn. (3) is given by

$$y(a, m, x_c, y_c) = S_1(a, m, x - x_c) + S_2(a, m, x - x_c) + y_c. \quad (5)$$

With  $\hat{t} = -\left(\frac{27m(x - x_c)}{2a}\right) + \sqrt{\left(\frac{27m(x - x_c)}{2a}\right)^2 + \frac{27}{a^3}}$ ,  $S_1 = \frac{-1}{3}\hat{t}^{1/3}$  and  $S_2 = \frac{1}{a}\hat{t}^{-1/3}$ .  $S_1$  dominates the lower end of the S-curves whereas  $S_2$  dominates the other part.

In Fig. 1, Eqn. (5) referred to as  $S_{a-m}$  curves and bell-curves of Eqn. (4) are compared with those of modified exponential function forms (Eqn. (1) and (2)). Originally introduced as an adjustment to  $y$ -axis in order to work with bounded dependent variable even for large values of the independent variable, Eqn. (3) has been used to classify the images of the fashion-MNIST dataset [12] and to model biological growth [10].

In the case of image classification, the parameter  $a$  acts as a regularizer and offers adaptive learning rate in a gradient descent based estimation. In [12], each of  $28 \times 28$  pixel value is represented as a component of  $\mathbf{x}$  and the input representation is a linear combination given by

$$w_0 + \sum_{i=1}^{n=784} w_i x_i = w^T \mathbf{x} \quad (6)$$

where  $w_i$ 's are weights. This input is activated with a two-parameter  $S_{a-m}$  curve for each category

$$ay^3 + y = m(w^T \mathbf{x}). \quad (7)$$

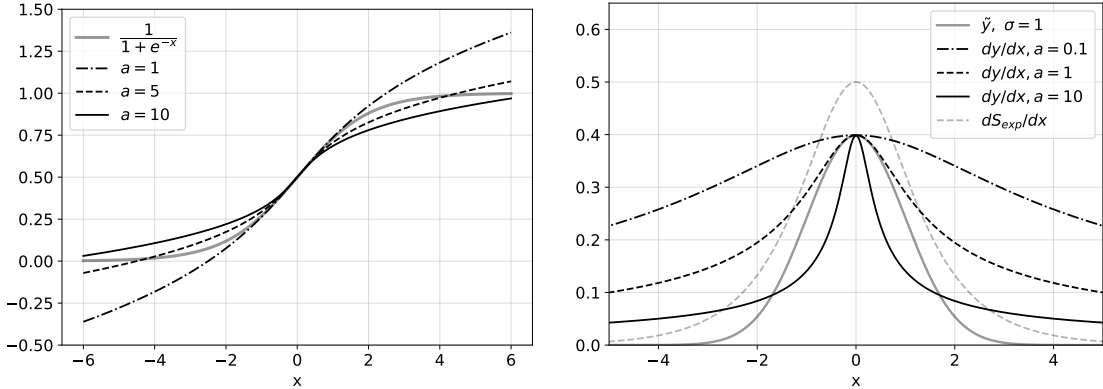
Thus instead of fixed hyperparametric values, we have parametric tuning of regularization and learning rate. This leads to quick convergence of logistic regression without Tikhonov[13] or lasso [14] regularization of weights with their learning rate set to unity. With Eqn. (7), the image classification accuracy is around 84% which means that 84% of Fashion-MNIST images fall under symmetric distribution described by Eqn. (4) when the images are represented as a linear combination of normalized pixel values. In the case of biological growth,  $a$  acts as a restriction parameter that introduces nonlinear restricting influences on linear growth with growth rate  $m$ . The model (Eqn. 3) fits the symmetric portions around the point of maximum growth which is  $(x_c, y_c)$ .

In Fig. 1, it can be noted that  $S_{a-m}$  curves do not offer the same curvatures of  $S_{\text{exp}}$  of Eqn. (1) or  $\tilde{y}$  (Eqn. (2)). Of course, the nonlinearity of exponential functions is unmatched with a simple parametric algebraic expression (Eqn. (3)) alone. So the natural choice would be to introduce more nonlinear terms in Eqn. (3) which may lead to a power series in  $y$  and more parameters as coefficients of high powers of  $y$ . Instead of such a complicated procedure, in the following section, we simply superpose various  $S_{a-m}$  curves with different origins (or point of inflections) and fit the superposition on the  $S_{\text{exp}}$  curve and the Gauss error function and obtain  $\tilde{y}$  as its derivative.

## 2 Superposition of $S_{a-m}$ curves

From Eqn. (3), we make the following observations and decide upon the superposed form.

1. Within data, there can be large variations in slope values yet a system under study is bounded and remains measurable. Even with large variations in  $m$ ,  $a$  parameterizes the nonlinear adjustment to  $y$  that keeps  $y$  bounded. So,  $a$  can be considered as an adjustment parameter or a nonlinear parameter as it turns on nonlinearities in Eqn. (3).



(a) Comparison of  $(a, m)$ - S-curves with  $S_{\text{exp}}$  with  $m = 1/\sqrt{2\pi}$ . As  $a \rightarrow 0$  the distribution becomes  $m = 0.25$  and  $(x_c, y_c)$  as  $(0, 0.5)$  for various  $a$ . (b)  $m = 1/\sqrt{2\pi}$ . As  $a \rightarrow 0$  the distribution becomes uniform and as  $a \rightarrow \infty$  the distribution resembles a delta function.

Figure 1: S- and bell- shaped curves of modified exponential function and modified (singularly perturbed) straight lines.

2. A slowly varying nonlinear curve such as  $S_{a-m}$  has only one point of inflection. When there are large variations that requires special tools such as the exponential function, it is assumed that multiple points of inflection exist causing such variations.
3. Since  $m$  is the value of slope at the inflection point  $(x_c, y_c)$ , in order to fit different variations in  $x$ , we superpose  $S_{a-m}$  curves of different slopes at different inflection points under a common  $y-$  axis adjustment by fixing  $a$ .

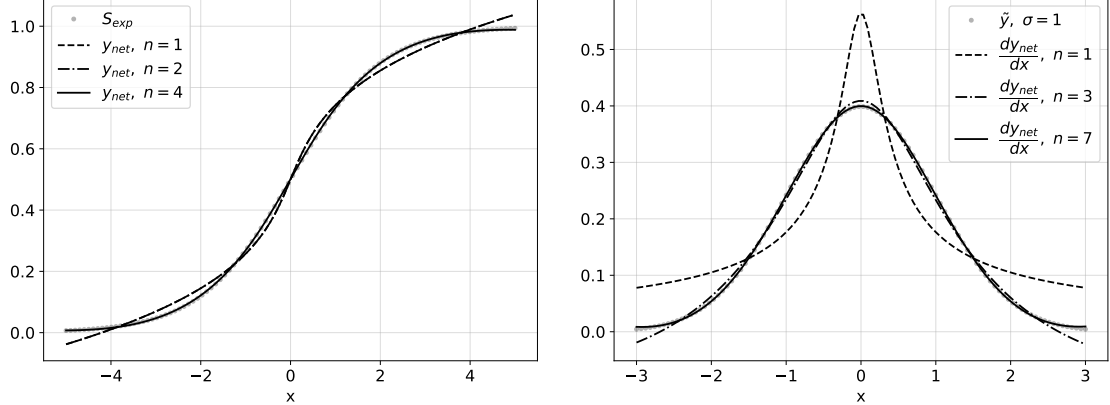
Therefore,  $S_{a-m}$  curves of different origins or inflection points are superposed in the following way

$$\begin{aligned} y_{\text{net}} &= \sum_{i=1}^n p_i y(a, m_i, x_{ci}, y_{ci}) \\ \Rightarrow y_{\text{net}} &= \sum_{i=1}^n p_i \left( \frac{m_i(x - x_{ci})}{1 + a(y_i - y_{ci})^2} + y_{ci} \right). \end{aligned} \quad (8)$$

where  $p_i$ 's are weights,  $m_i$  is the  $i^{\text{th}}$  slope with  $x_{ci}$  and  $y_{ci}$  as the origin coordinates or points of inflection. From (5),  $y_i \equiv y(a, m_i, x_{ci}, y_{ci}) = S_1(a, m_i, x - x_{ci}) + S_2(a, m_i, x - x_{ci}) + y_{ci}$ . The inflection points are chosen from the given data. This is done by choosing the midpoint of data points with the highest absolute slope values. This is implemented with python programming tool as follows:

```
#ams is the number of origins
grads=(ydata[1:]-ydata[:-1])/(xdata[1:]-xdata[:-1])
mxpts = np.argsort(np.abs(grads))[-ams:][::-1]
xcs = np.empty(ams); ycs = np.empty(ams)
for i in np.arange(ams):
    xcs[i] = (x[mxpts[i]]+x[mxpts[i]+1])/2
    ycs[i] = (y[mxpts[i]]+y[mxpts[i]+1])/2
```

We consider absolute slopes because  $m$  is allowed to take positive or negative values. We fit the linear combination on  $S_{\text{exp}}$  and  $\tilde{y}$  curves in Fig. 2a and 2b, respectively. The above superposition was first used to fit a bacterial growth dataset [15]. Here, we fit the superposition on the  $S_{\text{exp}}$  and  $\tilde{y}$  functions in Fig. 2a and 2b, respectively. To explain the fits in Fig. 2, consider two  $S_{a-m}$  curves that are superposed, for  $n = 2$



(a) Fitting superposed  $S_{a-m}$  curves on  $S_{\text{exp}}$ . Fits for  $n = 2$  and  $n = 4$  lie on top of each other.  
(b) Derivative of superposed  $S_{a-m}$  curves fitted on the Gauss error function.

Figure 2: Fitting superposed  $S_{a-m}$  curves on S- and bell-shaped curves obtained by modifying the exponential function. We get better fits as more  $S_{a-m}$  curves are added to the superposition.

we get

$$\begin{aligned}
y_{\text{net}} &= p_1 \frac{m_1(x - x_1)}{1 + a(y_1 - y_{c1})^2} + p_2 \frac{m_2(x - x_2)}{1 + a(y_2 - y_{c2})^2} \\
&= \frac{p_1 m_1 (x - x_1) (1 + a(y_2 - y_{c2})^2) + p_2 m_2 (x - x_2) (1 + a(y_1 - y_{c1})^2)}{(1 + a(y_1 - y_{c1})^2)(1 + a(y_2 - y_{c2})^2)}.
\end{aligned} \tag{9}$$

It can be seen that as we superpose more  $y_i$ 's there are higher powers of  $y_i$ 's in the  $y_{\text{net}}$  expression. Unlike higher order polynomials in  $x$ , the parametric estimation with  $S_{a-m}$  curves is bounded and we do not directly find the coefficient values of higher order terms. This way high orders with  $n = 11$  has been fitted on a growth data of a human male [16].

For  $n = 2$ , there are 5 parameters to be estimated they are  $a, p_1, m_1, p_2$  and  $m_2$ . Superposition of 3  $S_{a-m}$  curves leads to a 7-parametric fit. With  $n = 4$ , we fit a 9-parametric superposition and so on.

## 2.1 Measures from superposition

As shown in Fig. 2,  $S_{a-m}$  superposition has fit the sigmoid and the bell-curves. Although there are many parameters involved we characterize the fits by choosing two representative parameters  $a$  and  $m$ . Here,  $a$  can be estimated directly from the fit.  $m$  is the maximum slope value of the fitted curve or the peak value of the derived bell-curve, given by

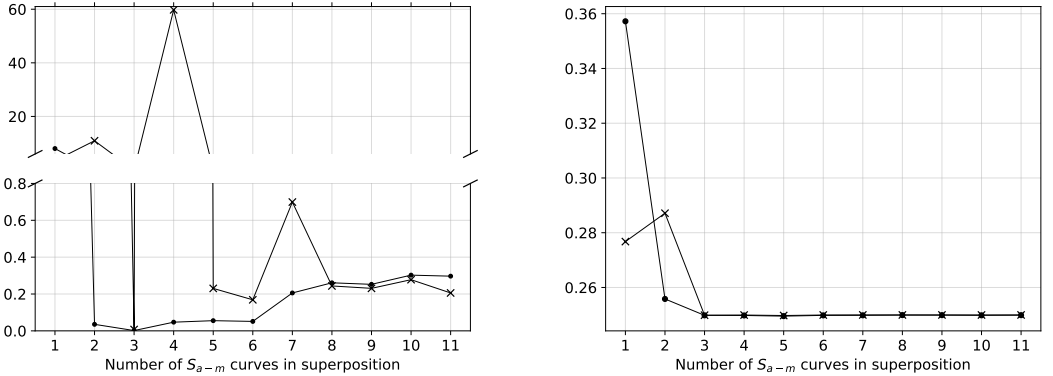
$$m = \left. \frac{dy_{\text{net}}}{dx} \right|_{\max}. \tag{10}$$

In this section, we will fit the superposition on  $S_{\text{exp}}$  for two different intervals of  $x$  and on the Gauss error function for two different initial conditions and analyze the estimated  $a$  and  $m$ . They are shown in Fig. 3 and 4. In Figs. 3 and 4, unlike  $a$ ,  $m$  converges to a precise value irrespective of initial condition or the interval size as long as the maximum slope lies within the interval. The differences in  $a$  are small when compared to unity. So, we can use the ratio  $m/(1 + a)$  as a measure to characterize a fit. This measure was introduced as an enzyme kinetic measure [17] to analyze protease activity on synthetic peptide substrates.

The other measure to characterize a fit is given by

$$\frac{|\sum_{i=1}^n p_i m_i - m|}{m}. \tag{11}$$

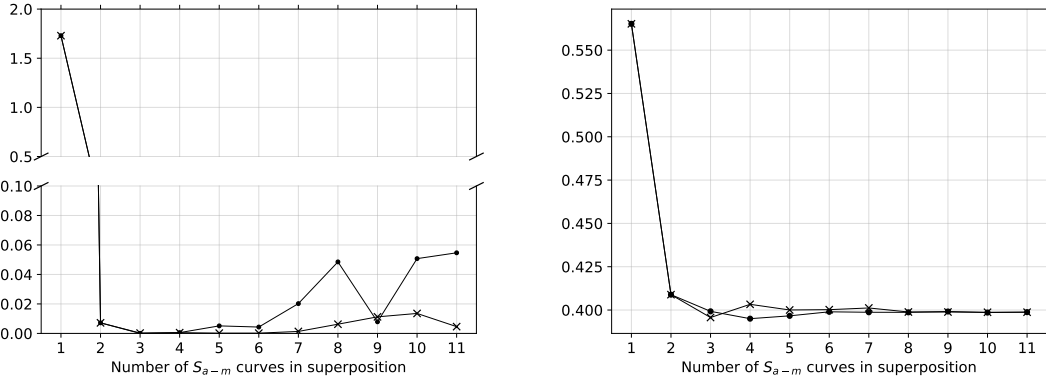
$\sum_{i=1}^n p_i m_i$  is  $dy_{\text{net}}/dx$  with the nonlinearities turned off (keeping  $a = 0$ ), while  $m$  depends on all the parameters including  $a$ . So, the above measure reflects the role of nonlinearities in the fit, hence this



(a) Estimation of  $a$  stabilizes to some extent as  $n$  increases.

(b) The maximum slope value  $m$  converge to a more accurate estimation as  $n$  increases.

Figure 3: Variation of parameters  $a$  and  $m$  based on the fits on  $S_{\text{exp}}$  for two different intervals  $x \in [-3, 3]$  (shown as ‘ $\times$ ’) and  $x \in [-5, 5]$  (shown as ‘ $\bullet$ ’) with  $n$  as the  $x$ -axis.



(a) Estimation of  $a$  stabilizes to some extent as  $n$  increases.

(b) The maximum slope  $m$  converge to a more accurate estimation as  $n$  increases.

Figure 4: Variation of parameters  $a$  and  $m$  based on the fits on Gauss error function whose derivative is  $\tilde{y}$  for two different initial conditions  $p_i = 1, m_i = 1$  (shown as ‘ $\times$ ’) and  $p_i = 0, m_i = \text{slope at } x_{ci}$  between data points (shown as ‘ $\bullet$ ’) with  $n$  as the  $x$ -axis.

measure is referred to as percentage nonlinearity measure. As shown in Fig. (5a), sigmoid function is more nonlinear on a wider interval  $x \in [-5, 5]$  than  $x \in [-3, 3]$  so the percentage nonlinearity of the former interval is higher than the later. However, the measure changes with the initial conditions of Gauss error fit shown in Fig. 5b. In Fig. 5c, the nonlinearity measure for sigmoid and Gauss error functions are compared for  $x \in [-3, 3]$  with same initial conditions. Gauss error function is observed to be more nonlinear than the sigmoid function in the same  $x$  interval.

To summarize this section, the measures available are

1. The height of the bell- curve  $m$ . We can precisely obtain this measure as we increase  $n$  without much dependence on initial conditions.
2. The ratio  $m/(1+a)$ . This measure works well as we increase  $n$ . However, uncertainty still exists due to fluctuations in  $a$ . Also. this measure is dependent on initial conditions.
3. Nonlinearity measure Eqn. (11). A curve is more nonlinear if it has a narrower peak. For example in

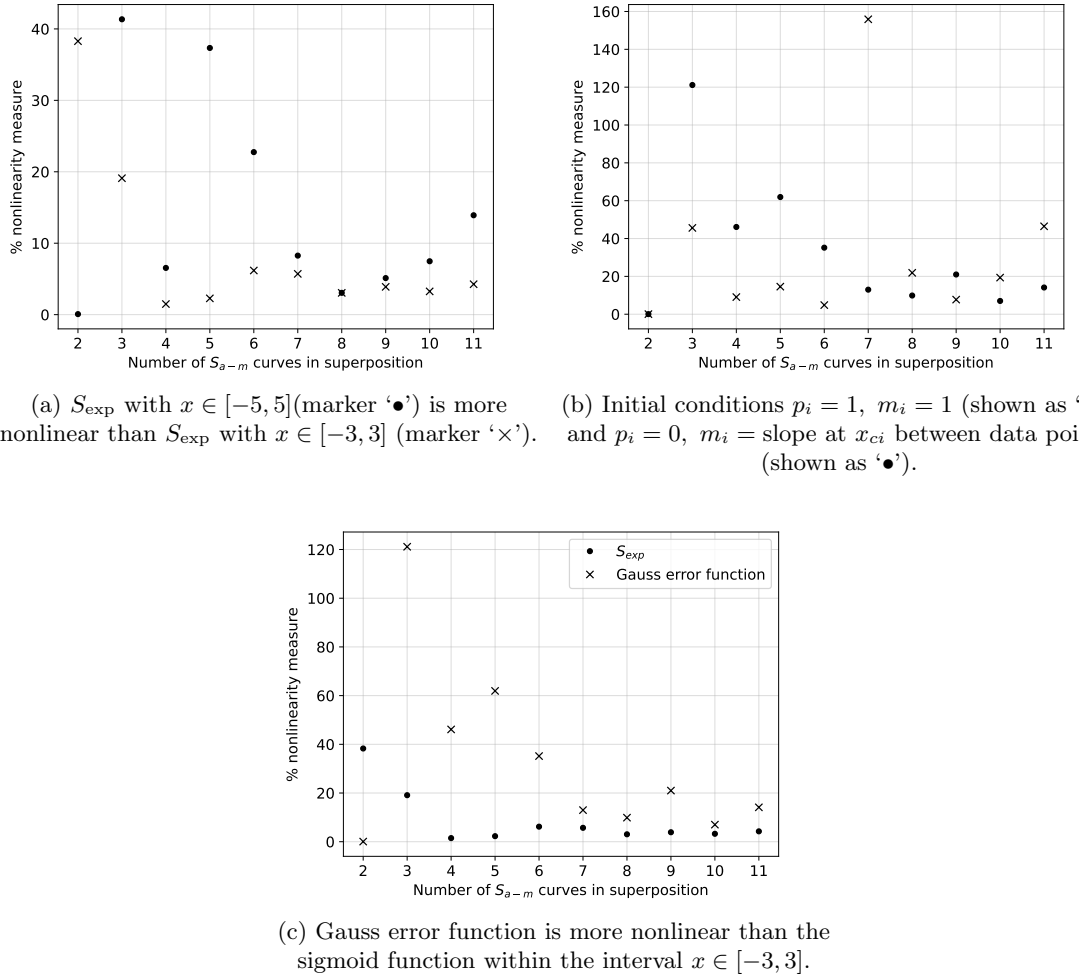


Figure 5: Percentage nonlinearity measures against the number of  $S_{a-m}$  curves in superposition for (a) sigmoid function under different  $x$  intervals (b) Gauss error function for different initial conditions (c) sigmoid and Gauss error function under the same initial conditions and  $x$  interval.

Fig. 2b, sigmoid bell-curve is less nonlinear than the normal distribution function as suggested by Fig. 5c.

While  $m$  is an absolute measure, the nonlinearity measure is a relative measure. The ratio  $m/(1 + a)$  is useful in ranking subsets of a dataset such as protease activity [17].

### 3 Pattern Recognition

As a nonlinear dynamic model the superposed form has fit biological growth data [11, 15] and chemical kinetic data [17]. In this section, we will use the  $S_{a-m}$  curve and its superposed form as a statistical model and fit the flower measurement data of iris plants. The dataset is publicly available in the UCI machine learning repository [18]. This is a balanced dataset containing four attributes sepal length, sepal width, petal length and petal width of flowers belonging to plant species *Iris setosa*, *Iris versicolour* and *Iris virginica*. There are 50 measurement values belonging to each species type.

The models are fitted on the cumulative density function and the corresponding probability curves are obtained as the derivatives of fitted models. The cumulative density function is obtained as follows:

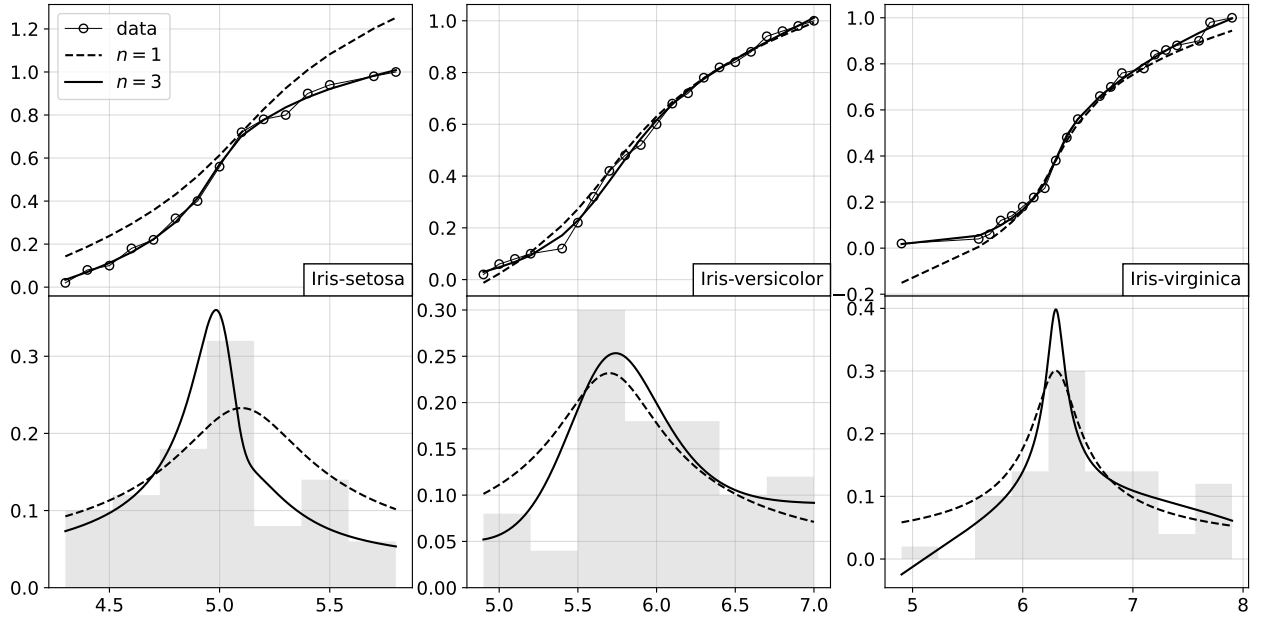


Figure 6: Fitted models on cumulative distributions of sepal length (in cm) of iris plants. The derived probability density curves are also shown below for each species. The parameter values for  $n = 1$  is shown in Table 1 and for  $n = 3$  in Table 2

Quantities	<i>Iris setosa</i>	<i>Iris versicolor</i>	<i>Iris virginica</i>
$a$	1.519780	2.295256	4.896959
$m$	1.086830	0.772745	0.901669
$x_c$	5.1cm	5.7cm	6.3cm
$y_c$	0.72	0.42	0.38
$\bar{m}$	0.232892	0.231823	0.300556

Table 1: Parameter values for  $n = 1$  in Fig. 6 with initial conditions  $a = 1$  and  $m = 0.1$ , with the constraint  $a > 1e - 9$ .

```
xax,cx = np.unique(np.sort(xdata),return_counts=True)
yax = np.cumsum(cx)/sum(cx)
```

The  $(xax, yax)$  plots and the fitted curves are shown on the top rows of Figs. 6 to 9. The models are given by

```
def sam(x,a,m):
hatt = (-27*x*m/2/a+np.sqrt(729*(x*m/2/a)**2+27/a**3))
S1 = -hatt**(1./3)/3
S2 = hatt**(-1./3)/a
return S1+S2
# Superposed sam curves
def sup_sam(params,xax,yax):
#params is a dictionary of parameters a,m1,p1,m2,p2 and so on
#xc,yc are lists of inflection point coordinates
supmod = 0
```

Quantities	<i>Iris setosa</i>	<i>Iris versicolor</i>	<i>Iris virginica</i>
$a$	1.496536	0.008575	0.000256
$p_1$	-0.136528	0.607929	-1001.161425
$m_1$	0.757782	1.911407	0.461323
$p_2$	0.808445	-0.640305	712.868633
$m_2$	2.722941	4.818308	0.648064
$p_3$	-0.171879	0.308483	0.003696
$m_3$	4.248980	8.906210	295.540954
$x_c$	5.4cm, 5cm, 5.1cm	5.5cm, 5.6cm, 5.7cm	6.4cm, 6.7cm, 6.3cm
$y_c$	0.9, 0.56, 0.72	0.22, 0.32, 0.42	0.48, 0.66, 0.38
$m$	1.679906	0.844489	1.195249
NL	18.591877	2.399107	1.929964
$\bar{m}$	0.359980	0.253347	0.398416

Table 2: Parameter values for  $n = 3$  in Fig. 6 with initial condition  $a = 1$ ,  $p_i = 1$  and  $m_i = 1$  with the constraint  $a > 1e - 9$ .  $\bar{m}$  represents probability density estimates.  $m$  is obtained using Eqn. (10)

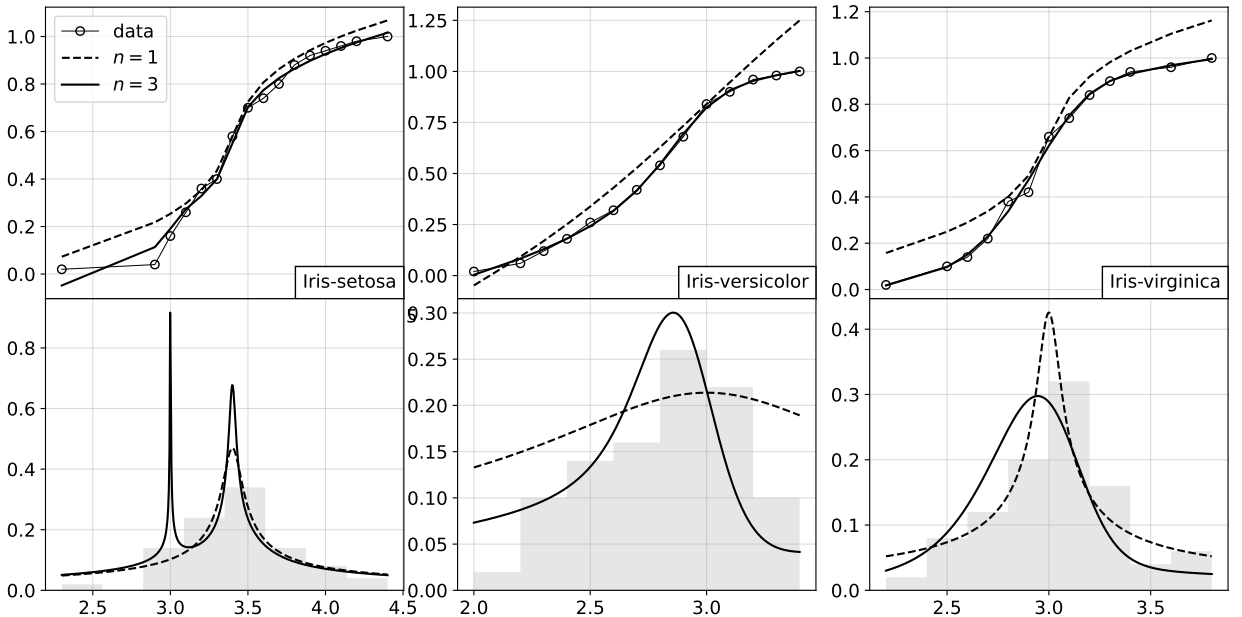


Figure 7: Fitted models on cumulative distributions of sepal width (in cm) of iris plants. The derived probability density curves are also shown below for each species. The parameter values for  $n = 1$  is shown in Table 3 and for  $n = 3$  in Table 4

```

a = params['a']; xc = params['xc']; yc = params['yc']
for i in range(1,len(xc)):
    supmod+=params['p'+str(i)]*(sam(xax-xc[i],a,params['m'+str(i)])+yc[i])
return supmod

```

We fit the above models using `lmfit` package [19]. The corresponding histograms on the bottom rows of Figs. 6 to 9 are obtained as follows:

```
import matplotlib.pyplot as plt
```

Quantities	<i>Iris setosa</i>	<i>Iris versicolor</i>	<i>Iris virginica</i>
$a$	11.216869	0.257162	9.462835
$m_1$	1.789357	1.068846	2.127825
$x_c$	3.4cm	3.cm	3.cm
$y_c$	0.58	0.84	0.66
$\bar{m}$	0.469706	0.213769	0.425565

Table 3: Parameter values for  $n = 1$  in Fig. 7 with initial condition  $a = 1$  and  $m = 0.1$  with the constraint  $a > 1e - 9$ .

Quantities	<i>Iris setosa</i>	<i>Iris versicolor</i>	<i>Iris virginica</i>
$a$	219.884500	225514.913420	0.000000
$p_1$	0.285454	-4070.946274	0.000900
$m_1$	13.519062	0.002175	-3222.157056
$p_2$	-0.694127	-9369.372072	0.001334
$m_2$	-0.191303	-0.002235	-1892.498683
$p_3$	-2.213338	4938.919811	-0.002209
$m_3$	-1.086762	-0.002283	-2898.034947
$x_c$	3cm, 3.5cm, 3.4cm	2.8cm, 2.9cm, 3cm	3.2cm, 2.8cm, 3cm
$y_c$	0.16, 0.7, 0.58	0.54, 0.68, 0.84	0.84, 0.38, 0.66
$m$	3.491381	1.501607	1.488202
NL	83.229072	45.780925	34.307505
$\bar{m}$	0.916487	0.300321	0.297640

Table 4: Parameter values for  $n = 3$  in Fig. 7 with initial condition  $a = 1$ ,  $p_i = 1$  and  $m_i = -1$  with the constraint  $a > 1e - 9$ .  $\bar{m}$  represents probability density estimates.  $m$  is obtained using Eqn. (10)

Quantities	<i>Iris setosa</i>	<i>Iris versicolor</i>	<i>Iris virginica</i>
$a$	2.109128	1.264663	1.495541
$m_1$	2.470337	0.866053	0.694955
$x_c$	1.5cm	4.5cm	5.1cm
$y_c$	0.74	0.72	0.32
$\bar{m}$	0.222330	0.259816	0.238270

Table 5: Parameter values for  $n = 1$  in Fig. 8 with initial condition  $a = 1$  and  $m = 0.1$  with the constraint  $a > 1e - 9$ .

```
c,b = np.histogram(xdata,bins='auto',density=True)
plt.stairs(c/sum(c),b,fill=True,color='k',alpha=0.1);
```

The derivatives of the models are obtained as follows

```
def sam_der(x,a,m):
    return m/(1+3*a*sam(x,a,m)**2)
def sup_der(x,params):
derval=0;
a=params['a'];xc = params['xc'];yc = params['yc']
for i in range(1,len(xc)):
    derval+=params['p'+str(i)]*params['m'+str(i)]/(1+3*a*sam(x-xc[i],a,params['m'+str(i)])**2)
```

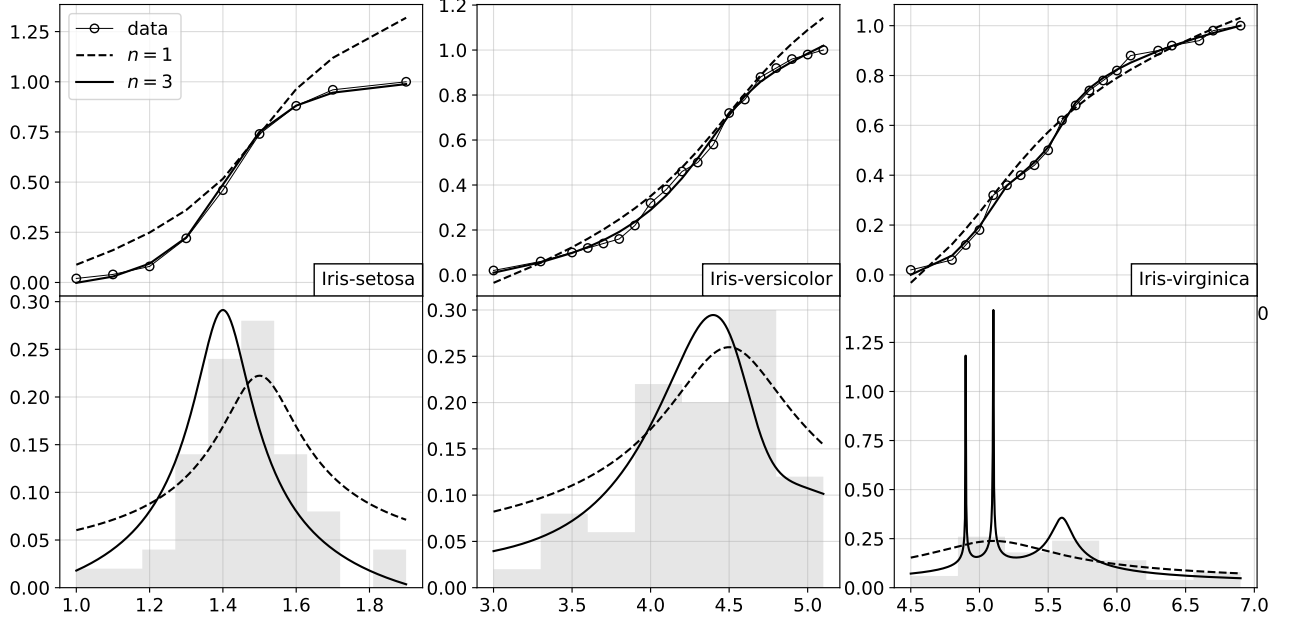


Figure 8: Fitted models on cumulative distributions of petal length (in cm) of iris plants. The derived probability density curves are also shown below for each species. The parameter values for  $n = 1$  is shown in Table 5 and for  $n = 3$  in Table 6

Quantities	<i>Iris setosa</i>	<i>Iris versicolor</i>	<i>Iris virginica</i>
$a$	0.142671	12457.557555	423.488765
$p_1$	-7.976545	149.711137	-0.113996
$m_1$	0.033544	-0.003129	-86.947406
$p_2$	-0.315143	-98.120756	-3.945396
$m_2$	-12.926374	0.011918	-0.240541
$p_3$	11.942307	277.277777	0.151272
$m_3$	-0.047720	0.008416	199.732348
$x_c$	1.6cm, 1.4cm, 1.5cm	4cm, 4.7cm, 4.5cm	4.9cm, 5.6cm, 5.1cm
$y_c$	0.88, 0.46, 0.74	0.32, 0.88, 0.72	0.12, 0.62, 0.32
$m$	3.236169	0.981885	4.128101
NL	0.001117	29.128698	894.998545
$\bar{m}$	0.291255	0.294565	1.415349

Table 6: Parameter values for  $n = 3$  in Fig. 8 with initial condition  $a = 1$ ,  $p_i = 1$  and  $m_i = -1$  with the constraint  $a > 1e - 9$ .  $\bar{m}$  represents probability density estimates.  $m$  is obtained using Eqn. (10)

```
return derval
```

and finally the probability density curves are plotted as

```
plt.plot(x,sam_der(x-xc,a,m)/sum(c))
plt.plot(x,sup_der(x,params)/sum(c))
```

$m$  is normalized as  $\bar{m}$  ( $\bar{m}=m/sum(c)$ ). The inflection points are chosen to be the most frequently observed measurements

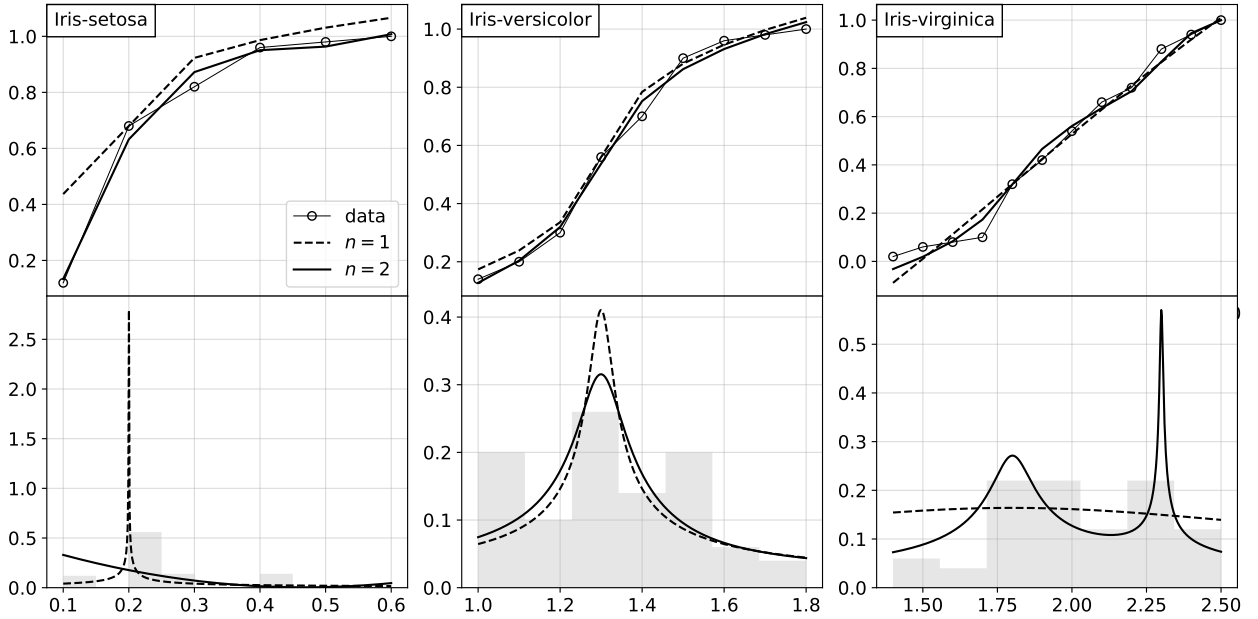


Figure 9: Fitted models on cumulative distributions of petal width (in cm) of iris plants. The derived probability density curves are also shown below for each species. The parameter values for  $n = 1$  is shown in Table 7 and for  $n = 3$  in Table 8

Quantities	<i>Iris setosa</i>	<i>Iris versicolor</i>	<i>Iris virginica</i>
$a$	3664.935912	11.989745	0.124025
$m_1$	529.168336	3.591652	1.043516
$x_c$	0.2cm	1.3cm	1.8cm
$y_c$	0.68	0.56	0.32
$\bar{m}$	26.458417	0.410475	0.163981

Table 7: Parameter values for  $n = 1$  in Fig. 9 with initial condition  $a = 1$  and  $m = 0.1$  with the constraint  $a > 1e - 9$ .

```
xax[np.argsort(cx)][::-1]
```

### 3.1 Results and discussions

Estimated values of parameters of fitted curves of Figs. 6 to 9 are provided in Tables 1 to 8. The key discussions based on the fitted models are provided below:

1. **Sepal length:** For  $n = 1$  model, the  $a$  values in Table 1 reveal that *Iris virginica* bell-curve is more centered and less distributed. This is inferred from the high  $a$  values which results in a narrow peak as shown in Fig. 1b. However, when we consider  $n = 3$  model, the nonlinearity measure NL in Table 2 is highest for *Iris setosa* data. This may be because the bell-curves of *Iris versicolor* and *Iris virginica* data are more evenly distributed with wider  $x$ -intervals. Hence, the NL values are less than *Iris setosa* data which has a skewed bell-curve in Fig. 6. *Iris setosa* data has a very narrow range of sepal length with a peak at around 4.9cm. It can be noted that  $n = 1$  model does not fit well for *Iris setosa* sepal length measurements for the chosen inflection point. However,  $n = 3$  reveals the actual inflection point and fits well for *Iris setosa* values.

Quantities	<i>Iris setosa</i>	<i>Iris versicolor</i>	<i>Iris virginica</i>
$a$	0.000334	458900.842161	$1.38 \times 10^{-8}$
$p_1$	-11142.446584	91.102275	0.000006
$m_1$	1.796412	-0.001988	542267.203734
$p_2$	22184.395854	308.879028	0.000036
$m_2$	0.902318	0.009430	44873.328378
$x_c$	0.4cm, 0.2cm	1.5cm, 1.3cm	2.3cm, 1.8cm
$y_c$	0.96, 0.68	0.9, 0.56	0.88, 0.32
$m$	6.599631	2.760746	3.629776
NL	85.664366	1.058830	35.796550
$\bar{m}$	0.329982	0.315514	0.570393

Table 8: Parameter values for  $n = 3$  in Fig. 9 with initial condition  $a = 1$ ,  $p_i = 1$  and  $m_i = -1$  with the constraint  $a > 1e - 9$ .  $\bar{m}$  represents probability density estimates.  $m$  is obtained using Eqn. (10)

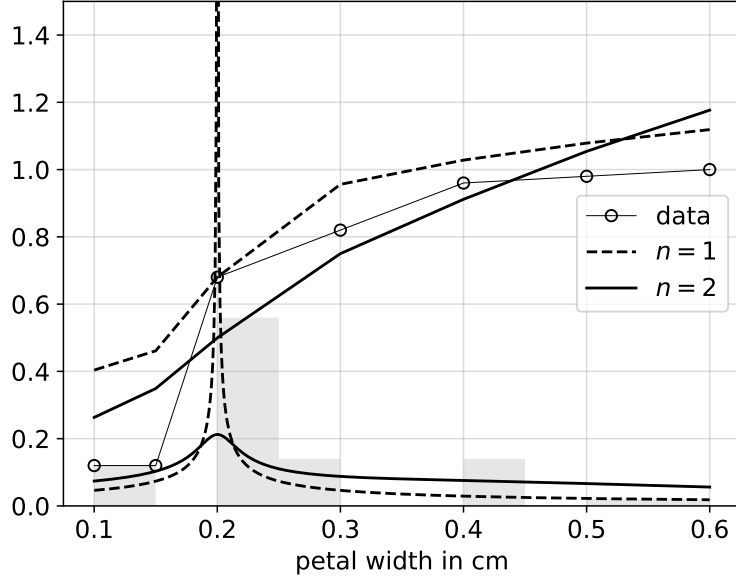


Figure 10: Fitted models on cumulative distributions of petal width (in cm) of Iris setosa after introducing a point at  $x = 0.15\text{cm}$ .

2. **Sepal width:** Considering the  $a$  values of Table 3, it is observed that the sepal width measurements of *Iris setosa* have a narrow peak centered around 3.4cm, however for *Iris versicolor* the distribution is more uniform and it has a minimal  $a$  value. From Fig. 7,  $n = 3$  model overfits *Iris setosa* measurements and shows an extra peak at 3cm. However,  $n = 3$  model fits well for *Iris versicolor* and *Iris virginica* measurements. The NL values in Table 4 suggests that the *Iris versicolor* sepal width data has a narrower distribution than that of *Iris virginica*.
3. **Petal length:** In Fig. 8,  $n = 3$  model fits well for *Iris setosa* data. The model however, overfits the petal length data of *Iris virginica*. The NL measure for *Iris setosa* fit is far less than that of *Iris versicolor*. This suggests that *Iris setosa* data is more evenly distributed than *Iris versicolor* data.  $n = 1$  model works well for data of *Iris versicolor* and *Iris virginica*.

4. **Petal width:** More than half of petal width data of *Iris setosa* is 0.2cm. So, the distribution is highly centered around 0.2cm in Fig. 9. However,  $n = 2$  model does not suggest a peak at 0.2cm. Also,  $n = 2$  model overfits *Iris virginica* data.  $n = 1$  model fits well on *Iris virginica* and suggests that petal width is distributed almost in a uniform manner for this species of iris plants. Both  $n = 1$  and  $n = 2$  do not provide us with the expected peak at 0.2cm for *Iris setosa* data. A better fit for  $n = 2$  is obtained in Fig. 10 by introducing a point at  $x=0.15$ cm with zero frequency. Now, we do get a peak at 0.2cm in the bell-shaped curve of Fig. 10 corresponding to  $n = 2$ .

5. From above points, the recognizable patterns are as follows:

- If sepal length is less than 5.5cm then sample is more likely an *Iris setosa* plant. If it is more than 6cm, then *Iris virginica* is the most likely category.
- Sepal widths are similar in all the three categories of iris plants.
- *Iris setosa* is more distinguishable using petal length and petal width features.
- If the petal length is around 5cm or more then *Iris virginica* is the most likely category.

The usefulness and drawbacks of  $S_{a-m}$  model and its superposition are presented in Table 9.

$n = 1$ ( $S_{a-m}$ curves)	$n > 1$ (superposed $S_{a-m}$ form)
2- parametric	5- (or more) parametric
$m$ is independent of $a$	$m$ depends on $a$
Robust estimates for various initial conditions	Sensitive to initial conditions
Sensitive to chosen point of inflection	Can be used to determine the point of inflection
Fits well for less nonlinear distributions and may underfit data	May fit highly nonlinear data and can result in overfitting of data
Applicable for unimodal distributions	Applicable for unimodal and multimodal distributions

Table 9: Comparison of  $S_{a-m}$  model and its superposition.

## 4 Conclusions

In this work we have presented an algebraic approach to model sigmoidal and bell-shaped patterns in data. This approach involves introducing a singular perturbation to the straight line equation using a positive parameter. The perturbation introduces a nonlinear adjustment to  $y$ -axis that keeps the straight lines bounded even for high slope values. The resulting curves, although nonlinear, are superposable with a common adjustment parameter. The superposed form can be used to fit highly nonlinear data of exponentially varying nature and can be used to quantify the nonlinearity of data. This ambitious attempt of using an algebraic approach has its drawbacks such as introduction of more parameters and sensitivity to initial conditions. This approach has been used to model a classical dataset of various flower measurements of *Iris* plant species and inferences have been made from the fitted model parameters.

## References

- [1] Kucharavy, D., and De Guio, R. (2011). Application of S-shaped curves. *Procedia Engineering*, 9, 559-572.
- [2] G. Cybenko. Approximation by superpositions of a sigmoidal function. *Mathematics of Control, Signals, and Systems*, 1989, 2 (4), pp.303-314. 10.1007/BF02551274. hal-03753170.
- [3] Hornik, K., Stinchcombe, M., and White, H. (1989), Multilayer Feedforward Networks are Universal Approximators, *Neural Networks*, Vol. 2, pp. 359-366.

- [4] Tsoularis, A., and Wallace, J. (2002). Analysis of logistic growth models. *Mathematical biosciences*, 179(1), 21-55.
- [5] Kyurkchiev, N., and Markov, S. (2015). *Sigmoid functions: some approximation and modelling aspects*. LAP LAMBERT Academic Publishing, Saarbrucken, 4.
- [6] Fekedulegn, D., Mac Siurtain, M.P., and Colbert, J.J. (1999). Parameter estimation of nonlinear growth models in forestry. *Silva Fennica* 33(4): 327–336.
- [7] Turner Jr, M. E., Bradley Jr, E. L., Kirk, K. A., and Pruitt, K. M. (1976). A theory of growth. *Mathematical Biosciences*, 29(3-4), 367-373.
- [8] Stahl, S. (2006). The evolution of the normal distribution. *Mathematics magazine*, 79(2), 96-113.
- [9] Taleb, N. N. (2020). Statistical consequences of fat tails: Real world preasymptotics, epistemology, and applications. arXiv preprint arXiv:2001.10488.
- [10] Shruti, I. S., and Vijay Prakash, S. (2025). A biological growth model using continued fraction of straight lines, bioRxiv doi:10.1101/2025.01.07.631841.
- [11] Shruti, I. S. (2025). A biological growth curve is a sum of two distinct S-curves, bioRxiv doi:10.1101/2025.02.06.636984.
- [12] Vijay Prakash S. (2024). Real-valued continued fraction of straight lines. arXiv preprint arXiv:2412.16191.
- [13] A. N. Tikhonov. On the stability of inverse problems. *Doklady Akademii Nauk SSSR*, 39(5): 195–198, 1943.
- [14] R. Tibshirani. Regression shrinkage and selection via the lasso. *Journal of the Royal Statistical Society. Series B. Methodological*, 58(1):267–288, 1996.
- [15] Shruti, I. S., and Vijay Prakash, S. (2025). Fitting multiple bacterial growth data using continued fraction of straight lines, bioRxiv doi:10.1101/2025.01.27.634991.
- [16] Shruti, I. S., and Vijay Prakash, S. (2025). Modeling Montbeillard's height data of a human male, bioRxiv doi:10.1101/2025.03.02.641023.
- [17] Suresh S, S VP. Analyzing enzyme kinetics using a growth model. *ChemRxiv*. 2025; doi:10.26434/chemrxiv-2025-57c99
- [18] Fisher, R. (1936). Iris [Dataset]. UCI Machine Learning Repository. <https://doi.org/10.24432/C56C76>.
- [19] Newville, M., Stensitzki, T., Allen, D. B., Rawlik, M., Ingargiola, A., and Nelson, A. (2016). LMFIT: Non-linear least-square minimization and curve-fitting for Python. *Astrophysics Source Code Library*, ascl-1606.